Title: Microwave dielectric properties and infrared reflectivity spectra analysis of two novel low-firing $AgCa_2B_2V_3O_{12}$ (Bnull=nullMg, Zn) ceramics with garnet structure

Authors: Junqi Chen, Ying Tang, Huaicheng Xiang, Liang Fang, Harshit Porwal, Chunchun Li

PII: S0955-2219(18)30383-2
DOI: https://doi.org/10.1016/j.jeurceramsoc.2018.06.021
Reference: JECS 11942

To appear in: *Journal of the European Ceramic Society*

Received date: 30-4-2018
Revised date: 4-6-2018
Accepted date: 8-6-2018

Please cite this article as: Chen J, Tang Y, Xiang H, Fang L, Porwal H, Li C, Microwave dielectric properties and infrared reflectivity spectra analysis of two novel low-firing $AgCa_2B_2V_3O_{12}$ (Bx202f;=x202f;Mg, Zn) ceramics with garnet structure, *Journal of the European Ceramic Society* (2018), https://doi.org/10.1016/j.jeurceramsoc.2018.06.021

Microwave dielectric properties and infrared reflectivity spectra analysis of two novel low-firing $AgCa_2B_2V_3O_{12}$ (B = Mg, Zn) ceramics with garnet structure

Junqi Chen[1], Ying Tang[1*], Huaicheng Xiang[1], Liang Fang[1, 3*], Harshit Porwal[4], Chunchun Li[1, 2*]

[1]State Key Laboratory Breeding Base of Nonferrous metals and specific Materials Processing, Guangxi universities key laboratory of non-ferrous metal oxide electronic functional materials and devices, College of Material Science and Engineering, Guilin University of Technology, Guilin, 541004, China

[2]College of Information Science and Engineering, Guilin University of Technology, Guilin, 541004, China

[3]Key laboratory of inorganic nonmetallic crystalline and energy conversion materials, College of Materials and Chemical Engineering, Three Gorges University, Yichang, 443002, China

[4]School of Engineering and Material Science, Queen Mary University of London, London E1 4NS, UK

[*]**Corresponding Author**: fanglianggl001@aliyun.com; tangyinggl001@aliyun.com; lichunchun2003@126.com

Abstract

Two Ag-containing microwave dielectric ceramics $AgCa_2B_2V_3O_{12}$ (B = Mg, Zn) with garnet structure were prepared through solid-state reaction method. Dense ceramics were obtained at low sintering temperatures, 665 °C for $AgCa_2Zn_2V_3O_{12}$ and 730 °C for $AgCa_2Mg_2V_3O_{12}$. Their microwave dielectric properties were

characterized for the first time and analyzed by means of packing fraction, bond valence, octahedral distortion, Raman spectra and infrared reflectivity spectra. Both compounds displayed high chemical compatibility with Ag electrodes. Additionally, thermally stable ceramics with near-zero temperature coefficients of resonance frequency (τ_f) were achieved by forming ceramic composites with $CaTiO_3$.

Keywords: Ceramics; Garnet structure; Dielectric properties; $AgCa_2B_2V_3O_{12}$

1. Introduction

Recently, microwave dielectric properties of garnet vanadates $A_3B_2V_3O_{12}$ have attracted extensive attention owing to their excellent dielectric performances and the potential applications in the low temperature co-fired ceramics (LTCC) technology. Some garnet vanadates exhibited low sintering temperatures (<960 ºC), low dielectric constants (ε_r), high quality factors (Q×f), and compositionally adjustable temperature coefficients of resonant frequency (τ_f) [1-8]. In comparison to the Al- and Si-based garnets that have high sintering temperatures (> 1300 ºC) [9], it is reasonable to propose that the low sintering temperature of garnet vanadates origins from the low melting temperature (~ 690 ºC) of vanadium oxide. Thus, it is of great interest to search for novel low-firing microwave dielectric materials from garnet vanadates. Fortunately, the structural complexity of garnet provides great possibilities for composition design with wide range of cations available for A/B sites (A presents an

8-coordinated position while B is an octahedral site) [10-12]. To date, however, the search for low-firing microwave dielectric materials in garnet vanadates is lacking in specific designing guidelines and are almost based on trial and error method. .

Based on the cation occupation in garnets given in supplementary Table S1, it could be summarized that the structural stability of garnet depends strongly on the effective ionic radius of the A-(r_A) and B-site (r_B) cations. A simple conclusion is drawn that the garnet structure can be stabilized when $0.92 < r_A < 1.51$ and $0.72 < r_B < 0.76$ [13]. In consideration of the ionic radius of Ag^+ (1.28 Å) and Ca^{2+} (1.12 Å) in A site while Mg^{2+} (0.72 Å) and Zn^{2+} (0.74 Å) occupying the B site, two garnet compounds $AgCa_2B_2V_3O_{12}$ (B = Mg, Zn) were proposed.

Besides, some AgO-rich ceramics have been recently reported with favorable microwave dielectric properties and low sintering temperature, e.g. $(Na_{1.2}Ag_{0.8})MO_4$ sintered at 410 ºC with ε_r = 8.1, Q×f = 44,800 GHz and τ_f= -82 ppm/ºC, $(AgBi)_{0.5}WO_4$ sintered at 580 ºC with ε_r = 35.9, Q×f = 13,000 GHz and τ_f= -69 ppm/ºC [14,15]. Therefore, it is expected that the proposed $AgCa_2B_2V_3O_{12}$ (B = Mg, Zn) ceramics might exhibit low sintering temperatures and good dielectric properties.

In this paper, $AgCa_2B_2V_3O_{12}$ (B = Mg, Zn) ceramics were prepared by the solid-state reaction methods. The microwave dielectric properties were characterized for the first time, and the structure and properties were investigated by means of packing fraction, bond valence, octahedral distortion, Raman spectra and infrared reflectivity spectra. Furthermore, the adjustment for the temperature coefficients of resonant frequency (τ_f) of $AgCa_2B_2V_3O_{12}$ (B = Mg, Zn) ceramics were also studied by

the addition of $CaTiO_3$ [16].

2. Experimental procedure

High-purity raw powders Ag_2O, $CaCO_3$, ZnO, MgO, and NH_4VO_3 (>99.0%, Guo-Yao Co. Ltd., Shanghai, China) were weighed according to the stoichiometry and ball-milled in alcohol medium for 4 h. After drying, calcination was carried out at 600 °C for 4 h in air. Subsequently, the calcined powders were re-milled for 4 h and polyvinyl alcohol (PVA) was added as a binder. The resultant powders were pressed into disks with 10 mm in diameter and 5-6 mm in height by uniaxial pressing under a pressure of 80 MPa. The green disks were heated to 550 °C for 2 h at a heating rate of 1.5 °C /min to remove the PVA. Finally, these specimens were sintered at various temperatures for 4 h.

X-ray diffraction (XRD) data collected by an X-ray diffractometer (CuKα1, 1.54059 Å, Model X'Pert PRO, PANalytical, Almelo, Holland) were used to identify phase purity. Rietveld refinements using FULLPROF were performed to analyze crystal structure. The apparent densities of the sintered ceramics were measured by the Archimedes' method. The microstructural images of the polished and thermally etched samples were recorded using a scanning electron microscope (SEM) (Model JSM6380-LV SEM, Jeol, Tokyo, Japan). In thermal etching, all samples were heated at 50°C below their sintering temperatures for 10 minutes. Composition analysis were performed using energy-dispersive spectroscopy (EDS, IE 350; INCA, Oxford, U.K.). The Raman spectra were recorded at room temperature by using a Raman spectrometer (Thermo Fisher Scientific DXR, America) with a 532 nm line in the

range of 100-1000 cm^{-1}. The permittivity and dielectric loss of $AgCa_2B_2V_3O_{12}$ ceramics were measured in the TE_{011} mode by Hakki and Coleman method [17] using the network analyzer (Model N5230A, Agilent Co., Palo Alto, California) at the frequency range of 10 MHz-40 GHz. The τ_f values were analyzed using a temperature chamber (Delta 9039, Delta Design, San Diego, CA) and calculated using the following equation:

$$\tau_f = \frac{f_2 - f_1}{f_1 (T_2 - T_1)} \qquad (1)$$

where, f_1 and f_2 were the resonant frequency of the dielectric resonator at temperature 25 °C and 85 °C, respectively.

Room-temperature infrared reflectivity spectra were measured using a Bruker IFS 66v FT-IR spectrometer (Bruker Optics, Ettlingen, Germany) on the infrared beam line station (U4) at the National Synchrotron Radiation Lab (NSRL), China. The infrared reflectivity spectra were analyzed by the harmonic oscillator model as follow:

$$\varepsilon^*(\omega) = \varepsilon_\infty + \sum_{j=1}^{n} \left(\frac{\omega_{pj}^2}{\omega_{oj}^2 - \omega^2 - j\gamma_j\omega} \right) \qquad (2)$$

where $\varepsilon^*(\omega)$ is the complex dielectric function, ε_∞ is the dielectric constant caused by the electronic polarization at high frequencies, γ_j, ω_{oj} and ω_{pj} are the damping factor, the transverse frequency, and plasma frequency of the j-th Lorenz oscillator, respectively, and n is the number of transverse phonon modes. The complex reflectivity $R(\omega)$ can be written as:

$$R(\omega) = \left| \frac{1 - \sqrt{\varepsilon^*(\omega)}}{1 + \sqrt{\varepsilon^*(\omega)}} \right|^2 \qquad (3)$$

3. Results and discussion

Fig. 1(a) shows XRD patterns of the $AgCa_2B_2V_3O_{12}$ (B = Mg, Zn) samples sintered at 665 ºC and 730 ºC, respectively. The peak positions obtained from the standard JCPDS cards (No. 024-1038 and No. 050-0393) are also given for indexing. By comparison, all the peaks matched well with the standard peaks, indicating single phase with cubic garnet structure in a space group of Ia-3d (230) was formed. Fig. 1(b) shows XRD pattern, SEM image, and EDS of the co-fired $AgCa_2B_2V_3O_{12}$ with 20 wt% silver sintered at 730 ºC as a representative. Only the peaks of $AgCa_2B_2V_3O_{12}$ and Ag were detected in the XRD patterns. SEM micrograph exhibited some larger Ag grains (~ 4-6 μm) distributed randomly among the $AgCa_2Mg_2V_3O_{12}$ matrix with smaller grains, further identified by the EDS analysis. Similar results were confirmed for the $AgCa_2Zn_2V_3O_{12}$ matrix. These results confirm that the $AgCa_2B_2V_3O_{12}$ ceramics are chemically compatible with silver electrodes at the sintering temperatures. To further confirm the phase purity and study their structural difference, Rietveld refinements using Fullprof software were performed based on the XRD data sets. The observed and calculated patterns are shown in Fig. 2 (a) and (b). Refinement data and crystal parameters are listed in Table 1. The good match with low residual factors confirm the reliability of the refinement. Schematic crystal structure of $AgCa_2B_2V_3O_{12}$ are shown in Fig. 2 (c) and (d). Mg and Zn cations occupy the $[BO_6]$ octahedral, while V cations are coordinated by four oxygen atoms, thus forming $[VO_4]$ tetrahedra. The neighboring tetrahedra and octahedral interconnect by corner-sharing, forming dodecahedra where A ions are located. As shown in Fig. 2 (d), Zn-O band lengths are much longer in comparison to the Mg-O band, and the distortion of $[ZnO_6]$ octahedral

101.3 ± 0.1 is more evident than that of [MgO_6] 36.8 ± 0.1 with different B-O band lengths and O-B-O band angles.

The bulk densities and relative densities of the $AgCa_2B_2V_3O_{12}$ (B = Mg, Zn) ceramics sintered at various temperatures are shown in Fig. 3. As the sintering temperature increased, the density of $AgCa_2Mg_2V_3O_{12}$ increased to a maximum value of 3.70 ± 0.01 g/cm^3 (~ 95.7 ± 0.2 % of the theoretical density) at 730 °C, whereas the density decreased slightly with the further increases of sintering temperature. $AgCa_2Zn_2V_3O_{12}$ exhibited a similar variation in density with sintering temperature, and the sample sintered at 665 ºC yielded the highest bulk density of 4.26 ± 0.01 g/cm^3 that is 94.2 ± 0.2 % of the theoretical density.

Fig. 4 (a-e) shows the SEM images recorded on the polished and thermally etched surfaces of $AgCa_2Mg_2V_3O_{12}$ ceramics sintered at different temperatures. As seen in Fig. 4(a), some visible pores were observed, which is consistent with the relatively low density of the ceramics sintered at 675 °C. The microstructure became denser as the sintering temperature increased while no significant change in the average grain size (1~ 2μm) was detected from 675 to 730 °C. However, abnormal grain growth was observed with further increase in sintering temperature to 745 °C, characterized by large grains (~ 100 μm) and cotton-shaped grains. This might be the consequence of liquid phase sintering at elevated temperatures which is related to the local composition heterogeneity. A homogeneous microstructure with average grain size about 1-3μm was developed when the ceramics were sintered at 730 °C. As

shown in Fig. 4(f), a dense microstructure with closely packed grains was obtained in the $AgCa_2Zn_2V_3O_{12}$ ceramic sintering at 665 °C.

The room-temperature Raman spectra of $AgCa_2B_2V_3O_{12}$ (B = Mg, Zn) ceramics are shown in Fig. 5. For the cubic garnet structure with a space group Ia-3d, the Raman activities can be summarized based on the group theory as follows:

$$\Gamma \text{ optic} = 3\ A_{1g} + 9\ E_g + 16\ T_{2g} \quad (4)$$

The vibrational models of $A_3B_2V_3O_{12}$ were reported to be divided into internal and external parts [18-20]. The internal vibrations were mainly assigned for the vibration of $[VO_4]^{3-}$ tetrahedron, whereas the external vibration contributed to the translational motion of cations and $[VO_4]^{3-}$. As observed, 16 emission bands fitted by the Gaussian-Lorentzian mode were detected. Below 250 cm^{-1}, the models were associated with the external translational motions of Ag^{+} and Ca^{2+} cations. In the range of 250-470 cm^{-1}, the Raman models were assigned for the rotational and translational motions of $[VO_4]^{3-}$. The peaks at the 500-800 cm^{-1} were ascribed to the bending vibration of $[VO_4]^{3-}$. The Raman models between 800 and 900 cm^{-1} were assigned for the asymmetric stretching vibration of $(VO_4)^{3-}$ unit. The modes 909 and 931 cm^{-1} for $AgCa_2Mg_2V_3O_{12}$ and 919 and 930 cm^{-1} for $AgCa_2Zn_2V_3O_{12}$ modes were related to the symmetric stretching of the $(VO4)^{3-}$ unit [21]. The different amounts Raman modes in the $AgCa_2B_2V_3O_{12}$ systems can be explained by the different ionic radii of B-site cations and the overlapping of the Raman peaks.

The variations in the microwave dielectric properties (ε_r, Q×f, and τ_f) of the $AgCa_2B_2V_3O_{12}$ (B = Mg, Zn) ceramics as a function of the sintering temperature are

shown in Fig. 6. It was found that both relative permittivity and quality factor exhibited slight dependence on the sintering temperature, similar to the variation tendency of the apparent density. However, the τ_f values did not significantly change as the sintering temperature increased. The optimum microwave dielectric properties were obtained with ε_r = 10.28 ± 0.1, Q×f = 43,000 ± 2000 GHz and τ_f = -69 ± 2.0 ppm/°C for $AgCa_2Mg_2V_3O_{12}$ at the sintering temperature of 730 °C and ε_r = 11.15 ± 0.1, Q×f = 26,930 ± 1500 GHz, τ_f = -95 ± 2.5 ppm/°C for $AgCa_2Zn_2V_3O_{12}$ sintered at the 665 °C.

It is well known that the microwave dielectric performances are influenced by the intrinsic factors, e.g. ionic polarizability, the anharmonic terms in the crystal's potential energy and the extrinsic factors related to densification, impurity, second phases and the lattice defects [5, 22]. As evidenced by the XRD analysis, the effects from impurity and second phases could be neglected. The dependence of dielectric properties manifests that the densification plays a crucial role in affecting the dielectric permittivity. In order to eliminate the contribution from the densification, the relative permittivity was corrected by the porosity-correction equation proposed by Bosman and Having [23, 24]. The corrected ε_r values, shown in Fig.6 (a), exhibit weak dependence on sintering temperature and fluctuate around ~ 10.7 ± 0.1 for $AgCa_2Mg_2V_3O_{12}$ and ~ 11.6 ± 0.1 for $AgCa_2Zn_2V_3O_{12}$. By comparison, the ε_r of $AgCa_2Zn_2V_3O_{12}$ is slightly higher than its Mg counterpart, which might be due to the higher ionic polarization of Zn^{2+} (2.04 $Å^3$) than Mg^{2+} (1.32 $Å^3$) based on the Clausius-Mosotti equation [14, 25]. On the other hand, $AgCa_2Mg_2V_3O_{12}$ possessed a

much higher Q×f value compared to $AgCa_2Zn_2V_3O_{12}$, which might be partly related to the lower relative density of as-sintered $AgCa_2Zn_2V_3O_{12}$ ceramics. In addition, the intrinsic loss can be reflected in terms of packing fraction. Generally, it is proposed that the increase in the packing fraction leads to a decrease in the lattice vibration, which then results in the decrease of intrinsic losses [26-29]. As exhibited in Table 1, the calculated packing fraction of $AgCa_2B_2V_3O_{12}$ (B = Mg, Zn) is 66.8 ± 0.01% and 66.6 ± 0.01%, respectively. Thus, the higher Q×f value of $AgCa_2Mg_2V_3O_{12}$ could be partly related to the higher packing fraction.

The bond valences of $AgCa_2B_2V_3O_{12}$ (B = Mg, Zn) with the general formula of $A_3B_2V_3O_{12}$ are shown in Table 1 calculated using the following equations:

$$V_i = \sum_j V_{ij} \qquad (5)$$

$$V_{ij} = \exp\left[\frac{R_{ij} - d_{ij}}{b}\right] \qquad (6)$$

Where R_{ij} is the bond valence parameter, d_{ij} is the length of a bond between atoms i and j, and b is a universal constant (0.37 Å) [30]. The bond valence of V_B and V_O are listed in Table 2. The larger τ_f value of $AgCa_2Zn_2V_3O_{12}$ might be ascribed to the smaller bond valance of V_B and V_O compared to those of $AgCa_2Mg_2V_3O_{12}$. Similar results were obtained in $Ba(Co_{1-x}Mg_x)_2(VO_4)_2$ [31], $LiMoVO_6$ [32] and Bi_2O_3-TiO_2-V_2O_5 system [33].

As the τ_f values of $AgCa_2B_2V_3O_{12}$ (B = Mg, Zn) ceramics are too large for practical application, efforts were carried out to improve the temperature stability of $AgCa_2B_2V_3O_{12}$ by forming composite ceramics with $CaTiO_3$ with a large positive τ_f value ~ +800 ppm/°C. The results are shown in Table 2 and a near-zero temperature

coefficient of resonant frequency (τ_f) ~ -2 ± 0.2 ppm/°C was achieved in $0.91AgCa_2Mg_2V_3O_{12}$-$0.09CaTiO_3$ ceramic, along with ε_r ~ 13.78 ± 0.1 and Q×f ~ 30,700 ± 1600 GHz. The $0.88AgCa_2Zn_2V_3O_{12}$-$0.12CaTiO_3$ sintering at 725 °C resulted in ε_r ~ 15.89 ± 0.1, Q×f ~ 19,600 ± 1200 GHz and a near-zero temperature coefficient of resonant frequency τ_f ~ +1 ± 0.2 ppm/°C.

Based on the classic harmonic oscillator model, the infrared reflectivity spectra were fitted to speculate the intrinsic microwave dielectric properties of $AgCa_2B_2V_3O_{12}$ (B = Mg, Zn) ceramics. The fitting results are shown in the Fig. 7 and Table 3. The dielectric permittivity at the high frequencies (ε_∞) were 2.41 ± 0.05 and 2.26 ± 0.05, and the extrapolated values (ε_0) were 7.47 ± 0.1 and 9.52 ± 0.1 for $AgCa_2Mg_2V_3O_{12}$ and $AgCa_2Zn_2V_3O_{12}$, respectively, which were lower than the measured ones using the TE_{011} method. It suggests that most of the dielectric contribution within microwave region was attributed to the absorptions of phonon oscillations in the infrared region.

The theoretical quality factor values of $AgCa_2B_2V_3O_{12}$ (B = Mg, Zn) can also be evaluated from the infrared reflectivity spectra by using the Lorentzian function [34, 35]. In the microwave frequency region ($\omega << \omega_{pj}$), the dielectric losses ($\tan\delta$) can be calculated by the following equation:

$$\varepsilon' = \varepsilon_\infty + \sum_{j=1}^{n} \frac{\omega_{pj}^2}{\omega_{oj}^2} = \varepsilon_\infty + \sum_{j=1}^{n} \Delta\varepsilon_j \qquad (7)$$

$$\tan\delta(\omega) = \frac{\varepsilon''}{\varepsilon'} = \omega \sum_{j=1}^{n} \frac{\Delta\varepsilon_j \gamma_j}{\omega_{oj}^2 (\varepsilon_\infty + \sum_{j=1}^{n} \Delta\varepsilon_j)} \qquad (8)$$

The theoretical Q×f value is 75,070 ± 3000 GHz (f = 12.08 ± 0.1 GHz) for $AgCa_2Mg_2V_3O_{12}$ and 58,970 ± 3000 GHz (f = 11.77 ± 0.1 GHz) for $AgCa_2Zn_2V_3O_{12}$.

These values are much higher than the measured ones using the TE_{011} method. The large deviation between the theoretical and experimental quality factors is due to the adverse influences from the extrinsic factors, such as density, secondary phase, grain size, etc. On the other hand, the fitting results give the optimum quality factor of $AgCa_2Mg_2V_3O_{12}$ ceramics and offer the possibility to further improve their Q×f values by optimizing the experimental processes to minimize extrinsic loss.

4. Conclusions

In this paper, $AgCa_2B_2V_3O_{12}$ (B = Mg, Zn) ceramics with garner structure were prepared by the conventional solid-state reaction method. The phase purity, crystal structure, packing fraction, bond valence, octahedral distortion and microwave dielectric properties were investigated. Raman and infrared reflectivity spectra were original to performing on the $AgCa_2B_2V_3O_{12}$ (B = Mg, Zn) ceramics. Excellent microwave dielectric properties were obtained in $AgCa_2Mg_2V_3O_{12}$ ceramic sintered at 730 °C for 4 h, with a permittivity of 10.28 ± 0.1, Q×f values 43,000 ± 2000 GHz, and a stable τ_f values around -69 ± 2.0 ppm/°C. The $AgCa_2Mg_2V_3O_{12}$ceramic sintered at 665 °C for 4 h also exhibited an excellent microwave dielectric properties with a ε_r ~ 11.15 ± 0.1, Q×f ~ 26,930 ± 1500 GHz and τ_f ~ -95 ± 2.5 ppm/°C. From the XRD, SEM and EDS analysis, the $AgCa_2X_2V_3O_{12}$ ceramics showed good chemical compatibility with Ag electrode, which makes it a promising candidate for LTCC application. Additionally, the temperature stability of $AgCa_2B_2V_3O_{12}$ were adjusted by forming composite ceramics with $CaTiO_3$. A near-zero temperature coefficient of resonant frequency (τ_f) ~ -2 ± 0.2 and +1 ± 0.2 ppm/°C were achieved in the

$0.91AgCa_2Mg_2V_3O_{12}$-$0.09CaTiO_3$ and $0.88AgCa_2Zn_2V_3O_{12}$-$0.12CaTiO_3$ ceramics, respectively.

Acknowledgments

This work was supported by Natural Science Foundation of China (Nos. 21561008, 51502047, and 21761008), the Natural Science Foundation of Guangxi Zhuang Autonomous Region (Nos. 2015GXNSFFA139003, 2016GXNSFBA380134, and 2016GXNSFAA380018), and Project of Scientific Research and Technical Exploitation Program of Guilin (2016010702-2, 20170225). The authors would also like to thank the administrators in the IR beamline workstation of National Synchrotron Radiation Laboratory (NSRL) for their help in the IR measurements.

References

[1] H.C. Xiang, L. Fang, X.W. Jiang, Y. Tang, C.C. Li, A novel temperature stable microwave dielectric ceramic with garnet structure: $Sr_2NaMg_2V_3O_{12}$, J. Am. Ceram. Soc. 99 (2016) 399-401.

[2] L. Fang, F. Xiang, C.X. Su, H. Zhang, A novel low firing microwave dielectric ceramic $NaCa_2Mg_2V_3O_{12}$, Ceram. Int. 39 (2013) 9779-9783.

[3] Y. Tang, X.W. Jiang, H,C. Xiang, C.C. Li, L. Fang, X.R. Xing, Two novel low-firing $Na_2AMg_2V_3O_{12}$(A = Nd, Sm) ceramics and their chemical compatibility with silver, Ceram. Int. 43 (2017) 2892-2898.

[4] H.C. Xiang, L. Fang, X.W. Jiang, C.C. Li, Low-firing and microwave dielectric properties of $Na_2YMg_2V_3O_{12}$ ceramic, Ceram. Int. 42 (2016) 3701-3705.

[5] L. Fang, C.X. Su, H.F. Zhou, H. Zhang, Novel low-firing microwave dielectric ceramic $LiCa_3MgV_3O_{12}$ with low dielectric loss, J. Am. Ceram. Soc. 96 (2013) 688-690.

[6] H. Luo, W.S. Fang, L. Fang, W. Li, C.C. Li, Y. Tang, Microwave dielectric properties of novel glass-free low temperature firing $ACa_2Mg_2V_3O_{12}$ (A = Li, K) ceramics, Ceram. Int. 42 (2016) 10506-10510.

[7] C.X. Su, L. Fang, Z.H. Wei, X.J. Kuang, H. Zhang, $LiCa_3ZnV_3O_{12}$: A novel low-firing, high Q microwave dielectric ceramic, Ceram. Int. 40 (2014) 5015-5018.

[8] H.C. Xiang, Y. Tang, L. Fang, H. Porwal, C.C. Li, A novel ultra-low temperature cofired $Na_2BiZn_2V_3O_{12}$, ceramic and its chemical compatibility with metal electrodes, J. Mater. Sci: Mater. Electron.28 (2017) 1508-1513.

[9] J.B. Song, K.X. Song, J.S. Wei, H.X. Lin, J. Wu, J.M. Xu, W.T. Su, Z.Q. Chen, Ionic occupation, structures, and microwave dielectric properties of $Y_3MgAl_3SiO_{12}$ garnet-type ceramics, J. Am. Ceram. Soc. 101 (2018) 244-251.

[10]M.T. Sebastian, R.Ubic, H. Jantunen, Low-loss dielectric ceramic materials and their properties, Int. Mater. Rev. 60 (2015) 392-412.

[11] G. Bayer, Vanadates $A_3B_2V_3O_{12}$ with Garnet Structure, J. Am. Ceram. Soc. 48 (1965) 600-605.

[12] R.R. Neurgaonkar, F.A. Hummel, Substitutions in the $Ca_2Na_6Al_6Si_6O_{24}(SO_4)_2$ hauyne structure, Mater. Res. Bull.11 (1976)61-65.

[13] R.D. Shannon, Dielectric polarizabilities of ions in oxides and fluorides, J. Appl. Phys. 73 (1993)348-366

[14] D. Zhou, J. Li, L.X. Pang, D.W. Wang, I.M. Reaney, Novel water insoluble $(Na_xAg_{2-x})MoO_4$ ($0 \leqslant x \leqslant 2$) microwave dielectric ceramics with spinel structure sintered at 410 degrees, J. Mater. Chem. C. 5 (2017) 6086-6091.

[15] D Zhou, W.B. Li, L.X. Pang, J. Guo, Z.M. Qi, T. Shao, Z.X. Yue, X. Yao, Sintering behavior and dielectric properties of ultra-Low temperature fired silver molybdate ceramics, J. Am. Ceram. Soc. 97 (2014) 3597-3601.

[16] A. Templeton, X. Wang, S.J. Penn, S.J. Webb, L.F. Cohn, N.M. Alford, Microwave dielectric loss of titanium oxide, J. Am. Ceram. Soc. 83 (2000) 95-100.

[17] B.W. Hakki, P.D. Coleman, A dielectric resonant method of measuring inductive capacitance in the millimeter range. IRE Trans Microwave Theory Technol. 8 (1960) 402-410

[18] H.T. Wu, Z.B. Feng, Q.J. Mei, J.D. Guo, J.X. Bi, Correlations of crystal structure, bond energy and microwave dielectric properties of $AZrNb_2O_8$ (A = Zn, Co, Mg, Mn) ceramics, J. Alloys Compds. 648 (2015) 368-373.

[19] U.A. Neelakantan, S.E. Kalathil, R. Ratheesh, Structure and Microwave dielectric properties of ultralow-temperature cofirable BaV_2O_6 ceramics, Eur. J. Inorg. Chem. 97 (2015) 1530-1533.

[20] G.G. Yao, C.J. Pei, P. Liu, J.P. Zhou, H.W. Zhang, Microwave dielectric properties of low temperature sintering $Ca_5Mn_4(VO_4)_6$, ceramics, J. Mater. Sci: Mater. Electron. 27 (2016) 7292-7296.

[21] F. Shi, H.L. Dong, Vibrational modes and structural characteristics of $(Ba_{(0.3)}Sr_{(0.7)})[(Zn_{(x)}Mg_{(1-x)})_{(1/3)}Nb_{(2/3)}]O_3$ solid solutions, Dalton. Trans. 40 (2011) 11591-11598.

[22] W. Lei, W.Z. Lu, J.H. Zhu, X.H. W, Microwave dielectric properties of $ZnAl_2O_4$-TiO_2spinel-based composites, Mater.Lett.61 (2007) 4066-4069.

[23] A.J. Bosman, E.E. Havinga, Temperature dependence of dielectric constants of cubic ionic compounds, Phys. Rev. 129 (1963) 1593-1600.

[24] C.C. Li, H.C. Xiang, M.Y. Xu, Y. Tang, L. Fang, Li_2AGeO_4 (A = Zn, Mg): Two novel low-permittivity microwave dielectric ceramics with olivine structure. J. Eur. Ceram. Soc.38 (2018) 1524-1528.

[25] M.T. Sebastian, Dielectric materials for wireless communication, Elsevier.2015.

[26] Y.G. Zhao, P. Zhang, Influence of Ta substitution for Nb in $Zn_3Nb_2O_8$ and the impact on the crystal structure and microwave dielectric properties, Dalton. Trans.45 (2016)11807-11816.

[27] E.S. Kim, B.S. Chun, H.K. Dong, Effects of structural characteristics on microwave dielectric properties of $(1-x)Ca_{0.85}Nd_{0.1}TiO_{3-x}LnAlO_3$(Ln= Sm, Er and Dy) ceramics, J. Eur. Ceram. Soc. 27 (2007) 3005-3010.

[28] C.C. Li, H.C. Xiang, Y. Tang, M.Y. Xu, J. Khaliq, J.Q. Chen, L. Fang, Low-firing and temperature stable microwave dielectric ceramics: $Ba_2LnV_3O_{11}$ (Ln = Nd, Sm), J. Am. Ceram. Soc. 101 (2018) 773-781.

[29] E.S. Kim, B.S. Chun, R. Freer, R.J. Cernik, Effects of packing fraction and bond valence on microwave dielectric properties of ABO (A: Ca, Pb, Ba; B: Mo, W) ceramics, J. Eur.Ceram. Soc. 30 (2010) 1731-1736.

[30] N.E. Brese, M. OKeeffe, Bond-valence parameters for solids, Acta Crystallogr.47 (1991) 192-197.

[31] C.H. Su, F.C. Lin, T.M. Chu, C.L. Huang, Structural characteristics and microwave dielectric properties of low-firing $Ba(Co_{1-x}Mg_x)_2(VO_4)_2$(x=0-1) ceramics, J. Alloys Compd. 686 (2016) 608-615.

[32] H.C. Xiang, C.C. Li, Y. Tang, L. Fang, Two novel ultralow temperature firing microwave dielectric ceramics $LiMVO_6$(M=Mo, W) and their chemical compatibility with metal electrodes, J. Eur. Ceram. Soc. 37 (2017) 3959-3963.

[33] D. Zhou, D. Guo, W.B. Li, L.X. Pang, X. Yao, D.W. Wang, I.M. Reaney, Novel temperature stable high-ε_r microwave dielectrics in the Bi_2O_3-TiO_2-V_2O_5 system, J. Mater. Chem. C.4 **(**2016) 5357-5362.

[34] J. Guo, D. Zhou, Y. Li, T. Shao, Z.M. Qi, B.B. Jin, H. Wang, Structure-property relationships of novel microwave dielectric ceramics with low sintering temperatures: $(Na_{(0.5x)}Bi_{(0.5x)}Ca_{(1-x)})MoO_{(4)}$, Dalton. Trans. 43 (2014) 11888-11896.

[35] K.Wakino, M. Murata, H. Tamura, Far infrared Reflection Spectra of $Ba(Zn,Ta)O_3$-$BaZrO_3$ dielectric resonator material, J. Am. Ceram. Soc. 69 (1986) 34-37.

Figure Captions

Fig. 1 X-ray diffraction patterns of $AgCa_2B_2V_3O_{12}$ (a), Backscattered electron image micrograph, and EDS analysis of the $AgCa_2Mg_2V_3O_{12}$ ceramic with 20 wt% silver powder (b).

Fig. 2 The Rietveld refined patterns of $AgCa_2Mg_2V_3O_{12}$ (a), $AgCa_2Zn_2V_3O_{12}$ (b), the structure diagram of $AgCa_2B_2V_3O_{12}$ (c), and units $[BO_6]$ octahedron and $[VO_4]$ tetrahedral of $AgCa_2B_2V_3O_{12}$ (B = Mg, Zn) (d).

Fig. 3 The bulk and relative density of $AgCa_2Mg_2V_3O_{12}$ and $AgCa_2Zn_2V_3O_{12}$ ceramics sintering at various temperatures.

Fig. 4 The SEM images of $AgCa_2Mg_2V_3O_{12}$ ceramics sintered at 675 °C (a), 690 °C (b), 705 °C (c), 730 °C (d), 745 °C (e) and $AgCa_2Zn_2V_3O_{12}$ ceramic sintered at best temperature 665 °C (f) for 4 h.

Fig. 5 The measured and fitted Raman spectra of $AgCa_2B_2V_3O_{12}$ (B = Mg, Zn) ceramics. The hollow red circles are measured values. Solid line represents the fitted values and the dashed line is the Gaussian-Lorentzian mode fitting.

Fig. 6 The microwave dielectric properties (ε_r, Q×f, and τ_f) of $AgCa_2Mg_2V_3O_{12}$ and $AgCa_2Zn_2V_3O_{12}$ ceramics as a function of the sintering temperature.

Fig. 7 Measured and calculated infrared reflectivity spectra and complex dielectric spectra of $AgCa_2B_2V_3O_{12}$ (B = Mg, Zn) ceramics (solid for fitting values and hollow symbol for measured values).

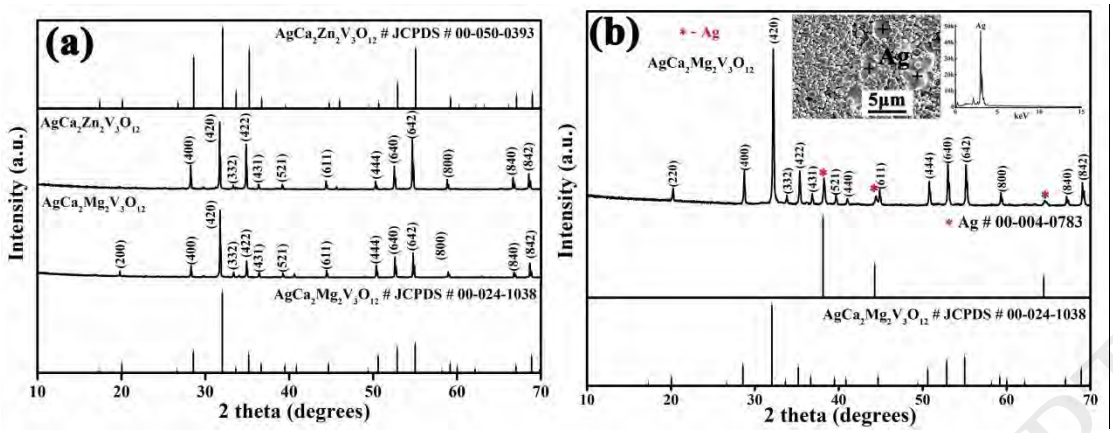

Fig. 1 (a) X-ray diffraction patterns of $AgCa_2B_2V_3O_{12}$ (B = Zn, Mg), (b) XRD, Backscattered electron image micrograph, and EDS analysis of the $AgCa_2Mg_2V_3O_{12}$ ceramic with 20 wt% silver powder.

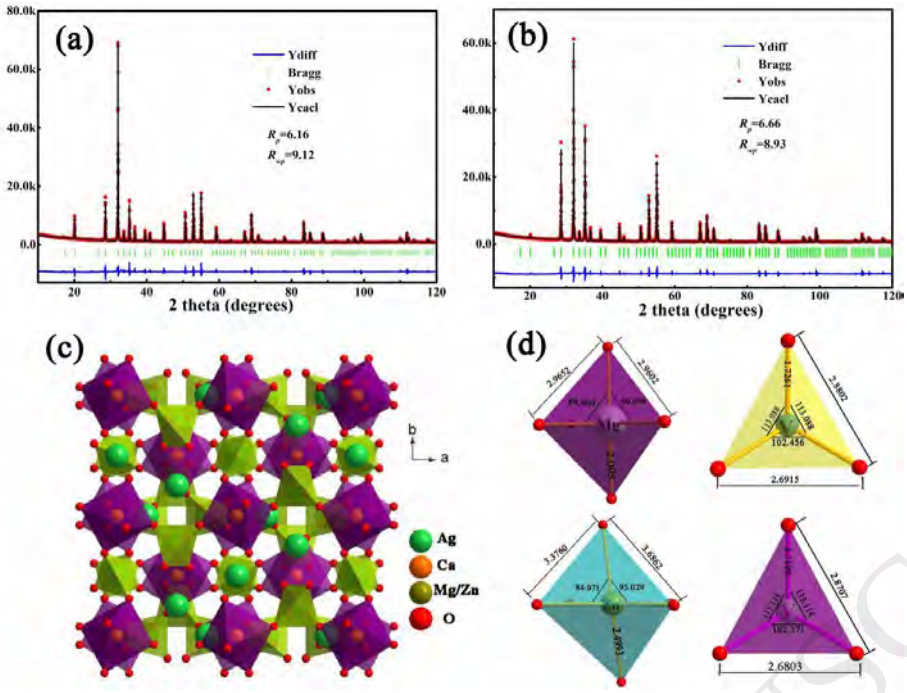

Fig. 2 The Rietveld refined patterns of $AgCa_2Mg_2V_3O_{12}$ (a), $AgCa_2Zn_2V_3O_{12}$ (b), the structure diagram of $AgCa_2B_2V_3O_{12}$ (c), and units $[BO_6]$ octahedron and $[VO_4]$ tetrahedral of $AgCa_2B_2V_3O_{12}$ (B = Mg, Zn) (d).

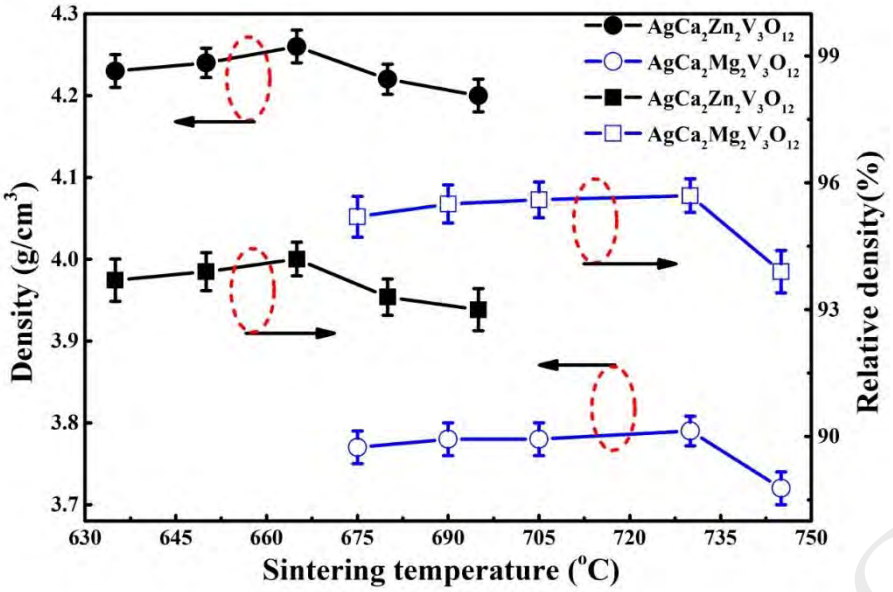

Fig. 3 The bulk and relative density of $AgCa_2Mg_2V_3O_{12}$ and $AgCa_2Zn_2V_3O_{12}$ ceramics sintering at various temperatures.

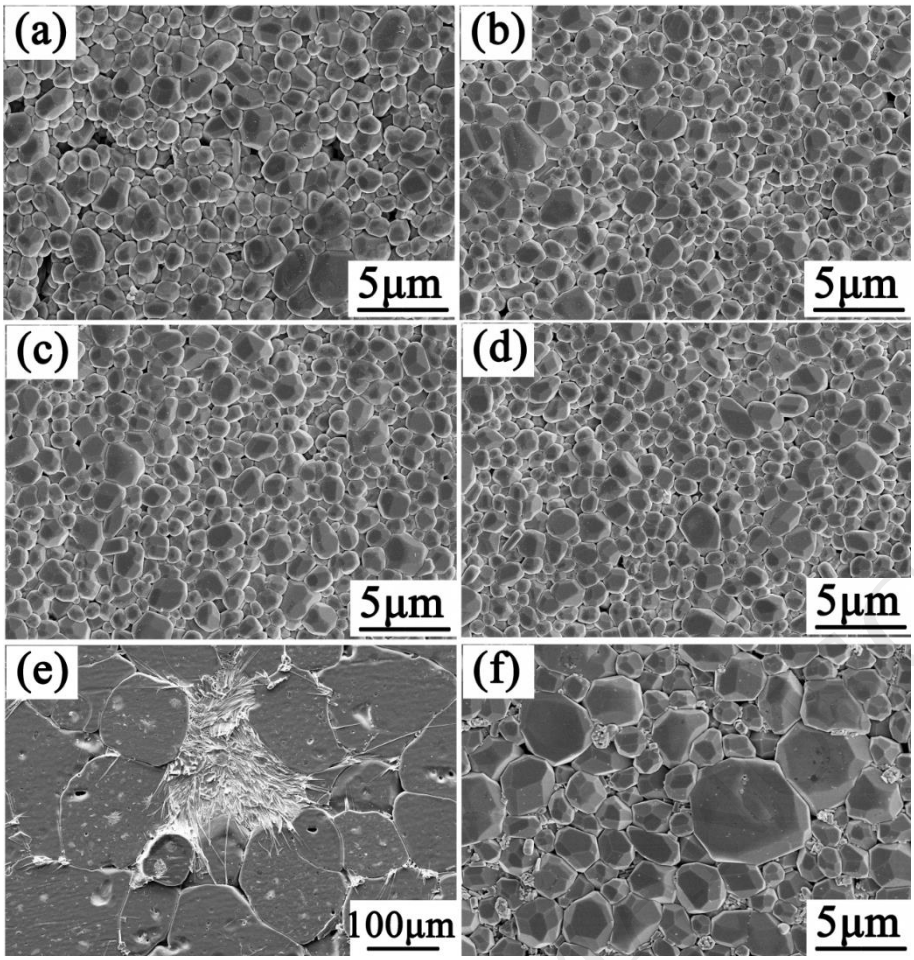

Fig. 4 The SEM images of $AgCa_2Mg_2V_3O_{12}$ ceramics sintered at 675 °C (a), 690 °C (b), 705 °C (c), 730 °C (d), 745 °C (e) and $AgCa_2Zn_2V_3O_{12}$ ceramic sintered at best temperature 665 °C (f) for 4 h.

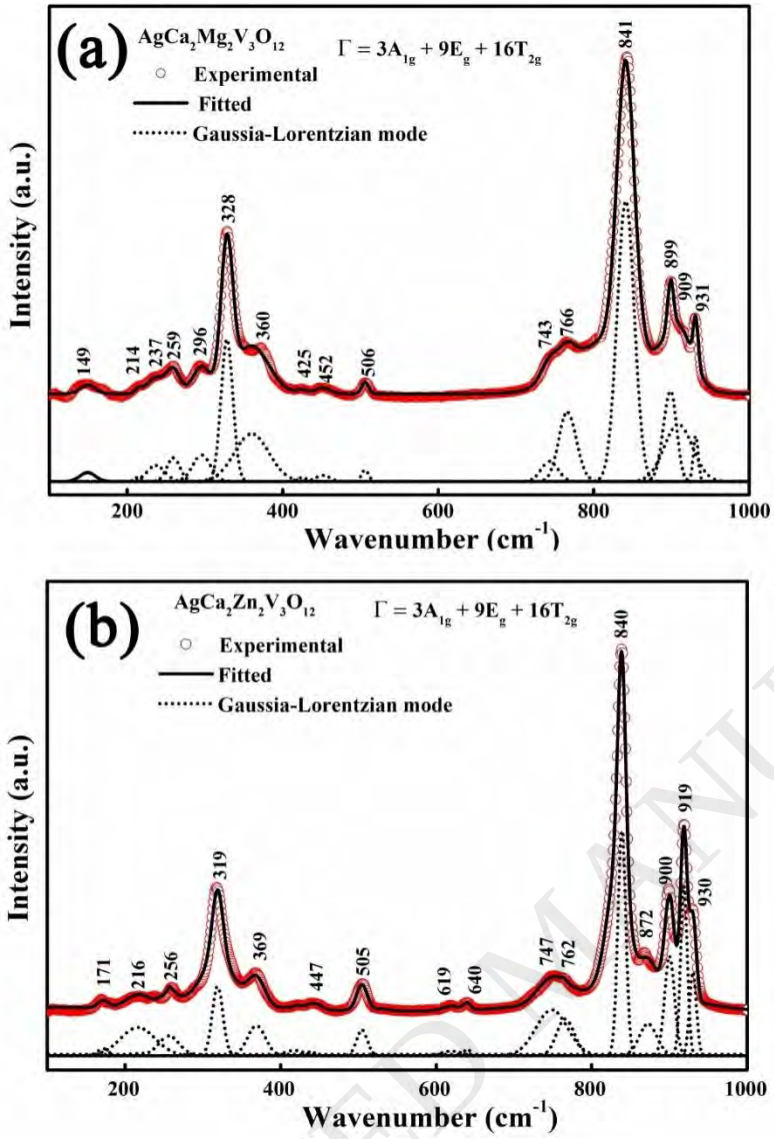

Fig. 5 The measured and fitted Raman spectra of $AgCa_2B_2V_3O_{12}$ (B = Mg, Zn) ceramics. The hollow red circles are measured values. Solid line represents the fitted values and the dashed line is the Gaussian-Lorentzian mode fitting.

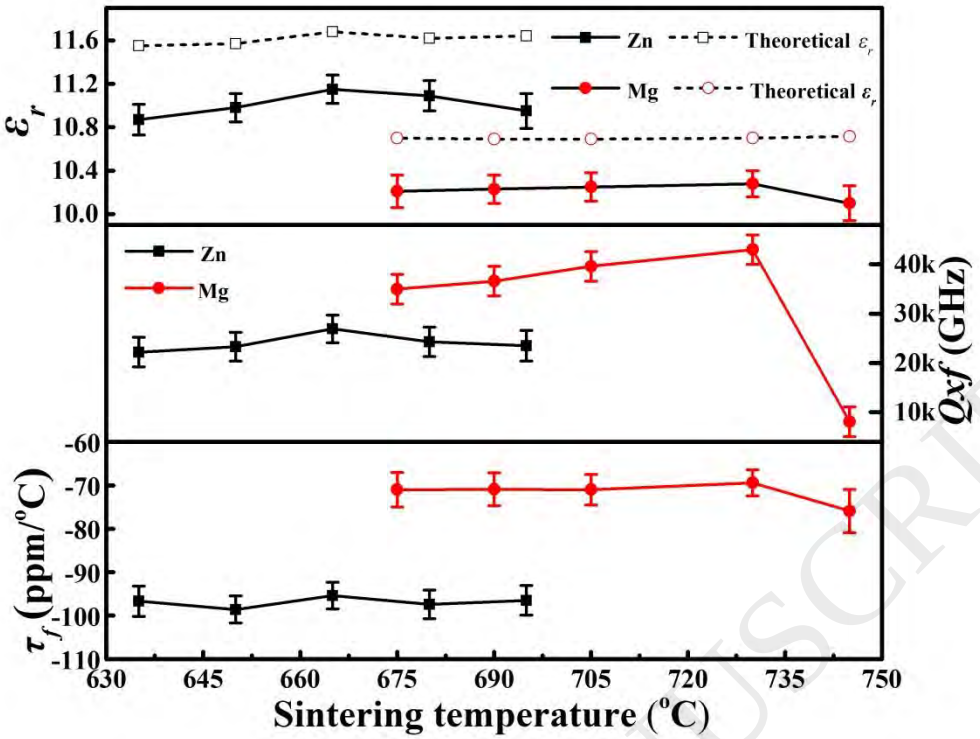

Fig. 6 The microwave dielectric properties (ε_r, Q×f, and τ_f) of $AgCa_2Mg_2V_3O_{12}$ and $AgCa_2Zn_2V_3O_{12}$ ceramics as a function of the sintering temperature.

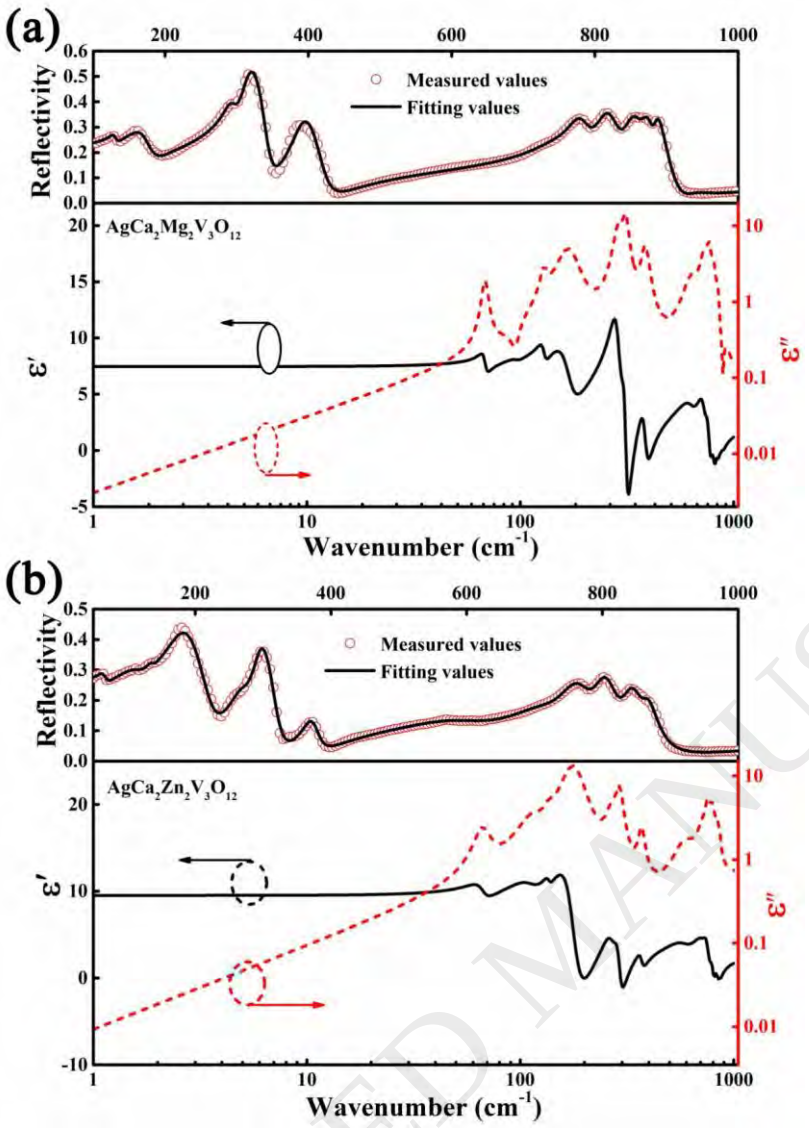

Fig. 7 Measured and calculated infrared reflectivity spectra and complex dielectric spectra of $AgCa_2B_2V_3O_{12}$ (B = Mg, Zn) ceramics (solid for fitting values and hollow symbol for measured values).

Tables:

Table 1 The Rietveld refinement dates, packing fraction and bond valence of $AgCa_2B_2V_3O_{12}$ (B = Mg, Zn)

Compounds	a (Å)	V (Å^3)	R_p(%)	R_{wp}(%)	$\rho_{(theoretical)}$ (g/cm^3)	Packing fraction (%)	V_B (Å)	V_O (Å)
$AgCa_2Mg_2V_3O_{12}$	12.4688 ± 0.0002	1938.54 ± 0.01	6.16 ± 0.01	9.12 ± 0.01	3.960 ± 0.001	66.8 ± 0.01	2.061 ± 0.001	1.999 ± 0.001
$AgCa_2Zn_2V_3O_{12}$	12.4943 ± 0.0002	1950.43 ± 0.01	6.66 ± 0.01	8.93 ± 0.01	4.492 ± 0.001	66.6 ± 0.01	1.981 ± 0.001	1.955 ± 0.001

Table 2 Microwave dielectric properties of (1-x) $AgCa_2B_2V_3O_{12}$ - $xCaTiO_3$ (B = Mg, Zn) composite ceramics

Composition	x value	S.T. (°C)	ε_r	Q×f(GHz)	τ_f(ppm/°C)
$AgCa_2Mg_2V_3O_{12}$	0	730	10.28 ± 0.1	43,000 ± 2000	-69.4 ± 2.0
	0.03	750	11.56 ± 0.1	39,850 ± 1800	-44.1 ± 1.5
	0.06	780	12.63 ± 0.1	36,800 ± 1700	-20.7 ± 1.0
	0.09	820	13.78 ± 0.1	30,700 ± 1600	-2.4 ± 0.2
	0.12	860	14.40 ± 0.1	27,600 ± 1500	+28.8 ± 1.1
$AgCa_2Zn_2V_3O_{12}$	0	665	11.15 ± 0.1	26,930 ± 1500	-95.4 ± 2.5
	0.04	680	12.47 ± 0.1	24,960 ± 1400	-61.2 ± 2.0
	0.08	700	14.56 ± 0.1	23,200 ± 1300	-27.0 ± 1.1
	0.12	725	15.89 ± 0.1	19,600 ± 1200	+1.3 ± 0.2
	0.16	780	18.05 ± 0.1	17,400 ± 1000	+44.1 ± 1.5

Table 3 Phonon parameters obtained from the fitting of infrared reflectivity spectra of $AgCa_2B_2V_3O_{12}$ (B = Mg, Zn)

$AgCa_2Mg_2V_3O_{12}$					$AgCa_2Zn_2V_3O_{12}$				
Mode	ω_{oj}	ω_{pj}	γ_j	$\Delta\varepsilon_j$	Mode	ω_{oj}	ω_{pj}	γ_j	$\Delta\varepsilon_j$
1	68.37	26.58	6.50	0.15	1	66.85	38.19	13.47	0.33
2	130.31	44.34	9.83	0.12	2	114.07	86.79	38.51	0.58
3	169.90	161.72	34.27	0.91	3	136.22	39.12	11.09	0.09
4	293.08	194.77	19.29	0.44	4	178.02	336.71	49.93	3.58
5	314.07	340.41	22.85	1.17	5	268.79	159.59	37.02	0.35
6	389.03	285.24	35.61	0.54	6	291.75	208.91	25.65	0.51
7	777.71	455.68	39.73	0.34	7	345.08	38.16	12.08	0.01
8	813.79	405.49	33.75	0.25	8	371.90	128.75	25.15	0.12
9	848.48	308.71	29.82	0.13	9	596.04	330.42	158.22	0.31
10	868.05	167.56	21.21	0.03	10	711.90	1301.58	93.62	0.18
11	883.87	106.81	13.46	0.01	11	758.39	380.56	52.19	0.25
					12	797.71	279.31	37.17	0.12
					13	837.55	212.90	34.30	0.06
					14	862.89	100.62	3.71	0.01
$\varepsilon_\infty = 2.41 \pm 0.05$; $\varepsilon_o = 7.47 \pm 0.1$					$\varepsilon_\infty = 2.26 \pm 0.05$; $\varepsilon_o = 9.52 \pm 0.1$				